Title: A qualitative assessment of a Modified Multilevel Converter topology M²LeC for lightweight low-cost electric propulsion

Authors: Paul H Riley[1]*, Obrad Dordevic[2], Keith Pullen[1], Liliana DeLilo[3], Massimo De Giorgio[3].

Abstract: A Cascade H Bridge (CHB) is evaluated for both electric vehicle motor traction control and off-vehicle charging against the PowerElectronicsUK Automotive Challenge for cost and mass for the year 2035. By combining the power electronics with batteries using low-voltage MOSFET transistors in a series cascade arrangement the cost and mass targets could be met 12 years earlier (in 2023 and 20 times lighter if an application specific integrated circuit (ASIC) is used.

A 200kW peak reference car was used to evaluate cost and mass benefits using four different topologies of power electronics.

Vehicle installation is shown to be simplified as only passive cooling is required removing the need for liquid cooling systems and the arrangement is inherently safe; no high voltages are present when the vehicle is stationary. The inherently higher efficiency of CHB increases vehicle range.

The converter with integrated batteries can also behave as an integrated on-board battery charger delivering additional off-vehicle benefits by removing the need for costly external chargers.

1. Introduction

For the large-scale acceptance of EVs, certain criteria have to be met, not least of which is the cost and mass of the Power Electronics (PE) used in traction high power ancillaries and fast battery chargers. In the aerospace sector, low vehicle mass is also of major importance to electric aircraft. The PowerElectronicsUK Automotive Challenge [1] has set a number of targets for the specific cost and mass of PE with the year 2035 targets being$3/kW and 50kW/kg. One of the strategies to meet these targets is system topology. This paper examines the suitability of a Multi-Level Converter (MLC) that house the PE with batteries to gain cost, mass and efficiency benefits over conventional topologies. Chang compared a conventional IGBT inverter with a silicon carbide and multi-level silicon inverter over a simulated driving range[2] and found a 2% – 3% improvement in the high rpm range and 3%-10% at lower operating speeds.

MLC in its various guises, Neutral-Point Clamped (or diode-clamped), Cascaded H-bridge, and Flying Capacitor are well-known topologies used for high voltage converters between AC and DC systems. A simplified drawing of the basic Cascaded H Bridge (CHB) concept is shown on Figure 1. The charge distribution in supercapacitors in a Modular-Multilevel-Converter (MMC) configuration was investigated in [3], while in [4] usage of switched individual Lithium cells in a series cascade configuration was proposed. MLC is a well-known topology used for high voltage converters between AC and HVDC systems[5] and more recently have been investigated for vehicle use. The charge distribution in supercapacitors

[1] City, University of London. School of Mathematics, Computer Science and Engineering. UK
*Corresponding author
[2] Liverpool John Moore University. UK
[3] University of Nottingham. UK

in a MLC configuration was investigated by Mukherjee and Tricoli [3] Figure 7 who also proposed using switched individual Lithium cells in a series cascade configuration [4]. Tolbert investigated two MLC topologies, CHB as a natural fit for all-electric drives and back-to-back diode-clamped (NPC) converter for hybrid vehicles where a source of ac voltage is available for motor control [6] for EVs and later proposed a solution for equalising state of charge between batteries [7]. Chang investigated a non-standard multi-level configuration with PWM signals [8] on what we describe in this paper as the Module In Control (MIC). A simplified drawing of the basic concept of Cascaded H-bridge (CHB) operation is shown in Tolbert proposed using a MLC for motor control [6] and later proposed a solution for equalising state of charge between batteries [7]. Chang improved on the waveform with PWM signals on the Module In Control (MIC) [8].

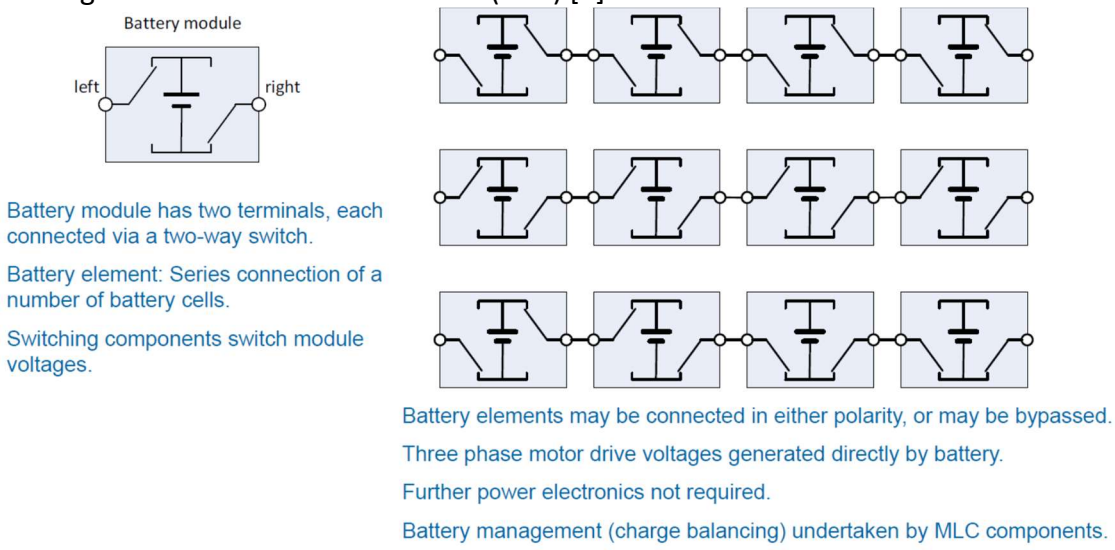

Figure 1, Simplified Multi-Level Inverter.

Until recently, these novel architectures were more expensive than centralised PE systems. However, with recent advances in miniature MOSFETs, distributed architectures are becoming more attractive, although relatively unknown outside academic circles. In this paper the term Cascaded H Bridge or CHB is used where the functions of motor control, battery management and battery charging are incorporated in a single set of MLC power electronics and the different functions controlled by software alone.
Two main drivers for electric vehicle manufacturers and hence parameters important to optimise are cost and mass: the topic of this paper.

1 Road Vehicle Topology

Road vehicles almost exclusively use “lumped” Power Electronics (PE) and battery modules as shown in Figure 3. The batteries are located in one area, motors in a second and PE in a third. More recent design have re-located these three elements on the floor and in between the road wheels but the basic topology remains the same. Cooling for all three modules is required usually by a liquid cooling system that adds cost and mass.
Figure 4 shows the modified topological arrangement. The batteries are segmented into 12 sections, three for each motor (assuming 4 wheel drive) and one for each motor phase. Each section comprises a multitude of low-voltage batteries with PE connected in series and using low-voltage high-current MOSFETs. The PE are assembled using micro-electronic

surface mount techniques to reduce costs. Distributing the PE has two installation advantages, firstly, the MLC is more efficient than conventional PE

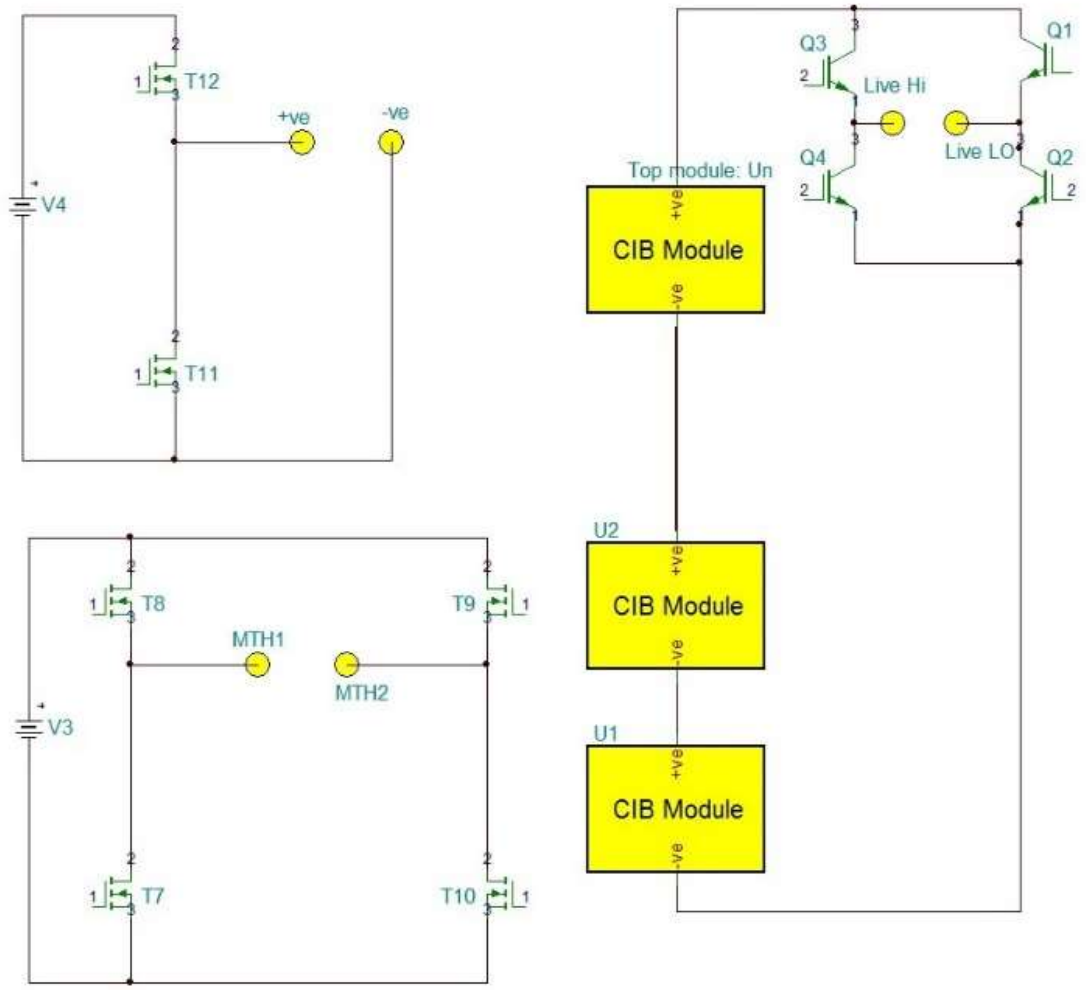

Figure 2, Module options, top left single I-bridge, the full cascade CIB is shown right in a section configuration. Bottom left H-bridge.

[2], [9] and secondly, being distributed no additional heat management is required; the heat is dissipated through the assembly casing. In a future paper we will also discuss how advances in Battery technology can also remove the heat management for batteries in such a distributed arrangement.

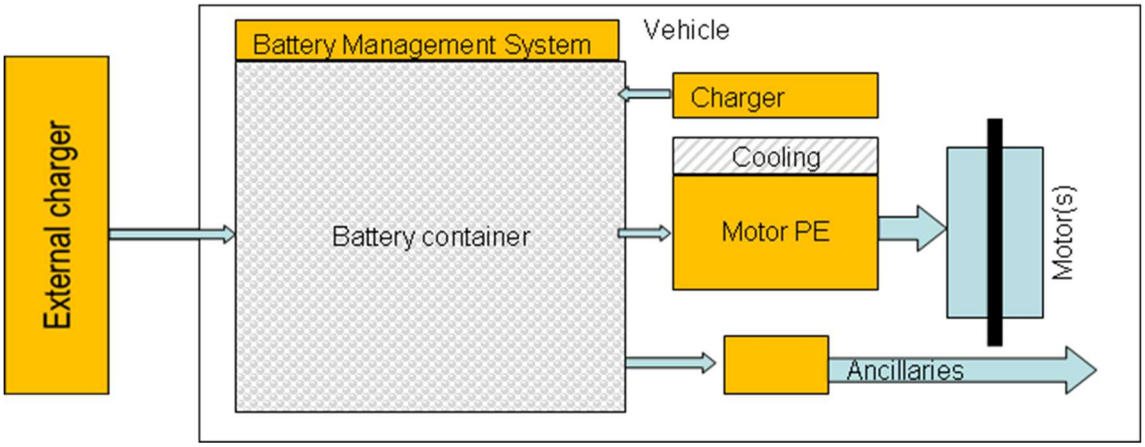

Figure 3. Typical automotive functional EV layout with chargers

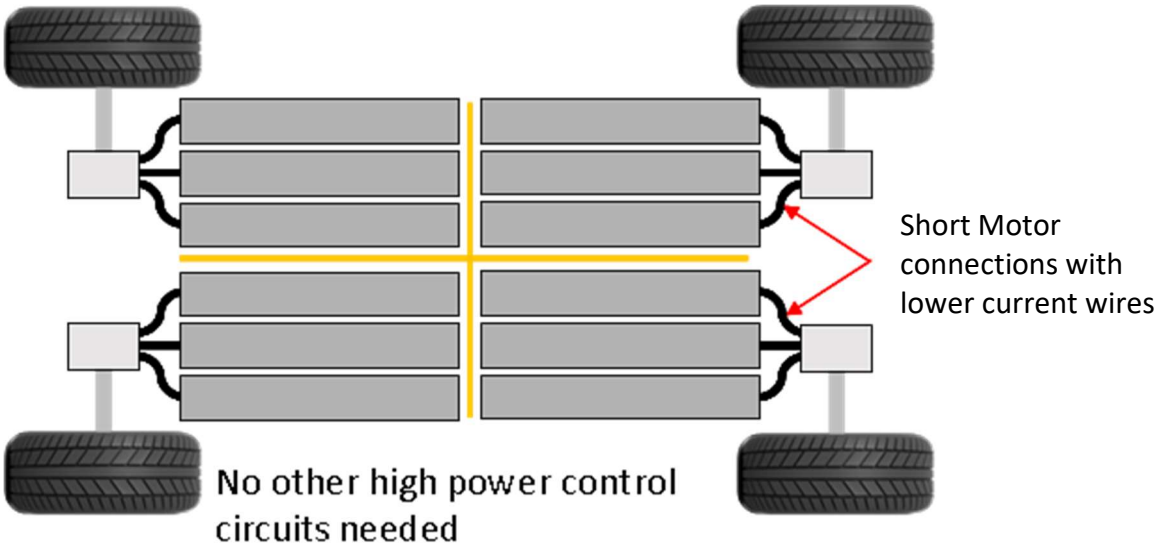

Figure 4, Distributed power electronics EV drivetrain.

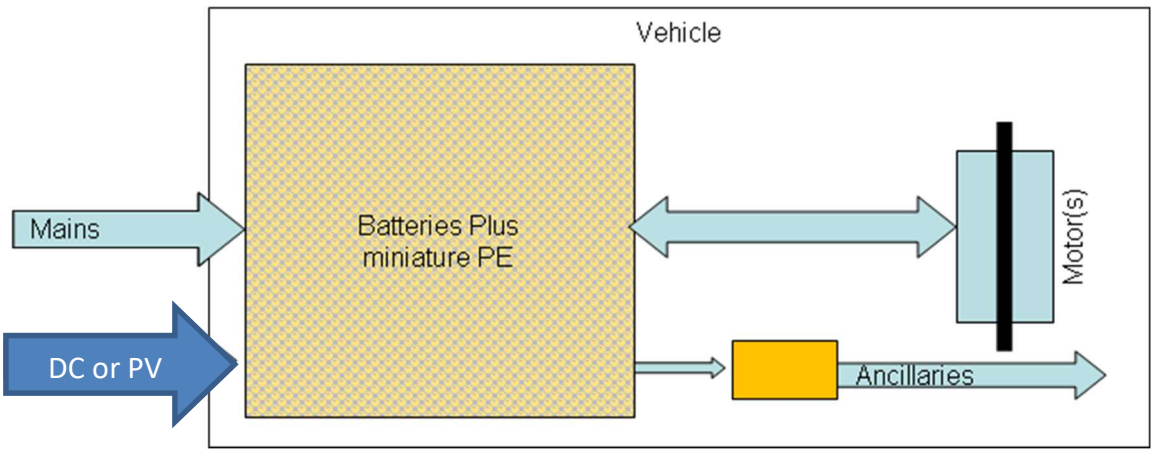

Figure 5, Functional description of CHB

The CHB Power electronic topology can also function as a battery charger without any additional Power electronics, and charging supply may be single or 3 phase AC, or DC as shown on Figure 5. In the DC configuration, if required, Maximum Power Point Tracking (MPPT) for solar cells can be achieved via a standard software algorithm [10].

2 Module configurations

The complete reference system used for comparisons is shown on Figure 6 for each of the four motors. One module in each phase controls the motor and receives signals from the vehicle control system. The battery management, vehicle and motor control costs and mass are excluded from the analyses below for a correct comparison with targets.

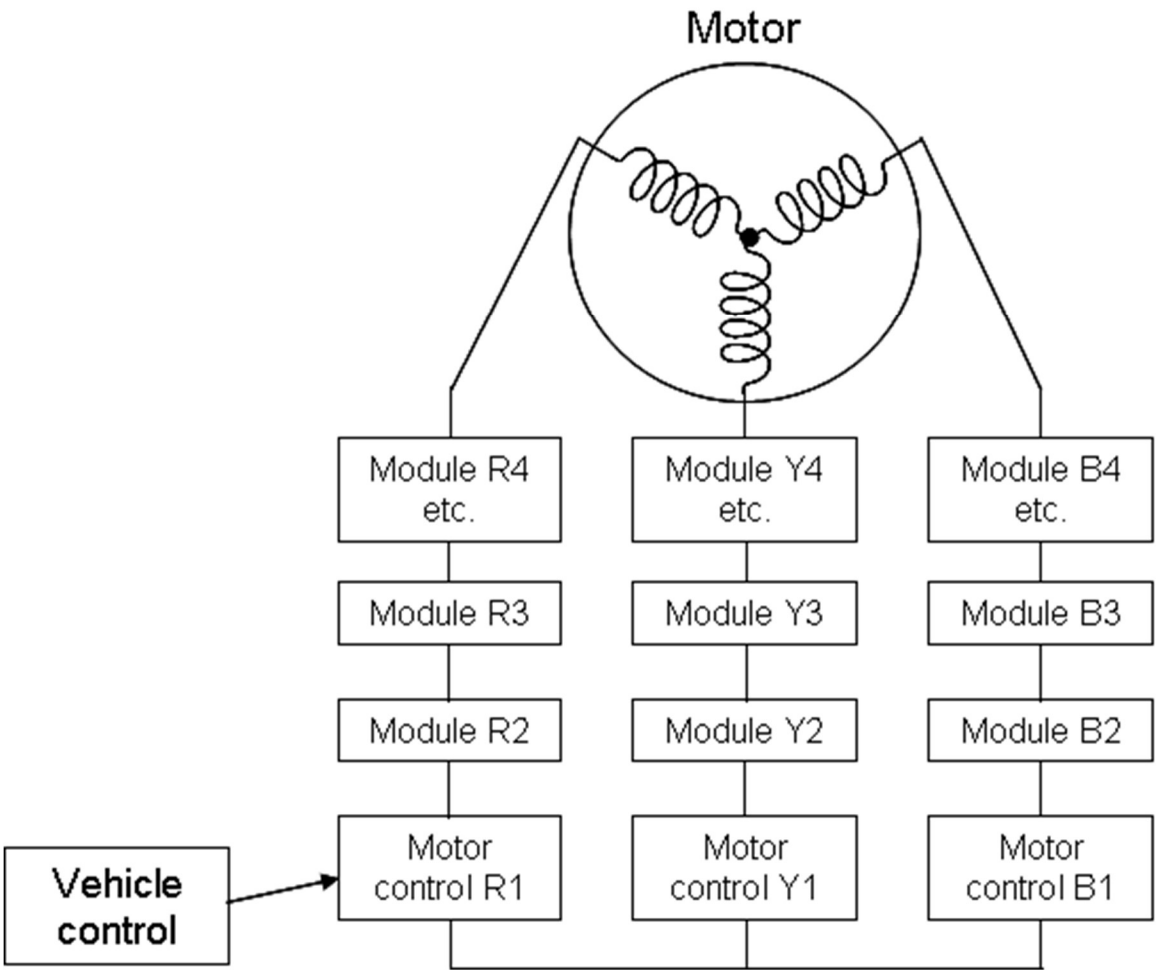

Figure 6, Reference system diagram

There are a number of benefits with the new topology shown on Figure 6; no high voltages are present when the vehicle is stationary (lower skilled maintenance personnel and first accident responders needed) and better optimisation of cost and mass as shown in the analysis paragraphs.

There are various configurations of PE available in the vehicle. As well as the standard two-level three-phase converter that is used in nearly all EVs nowadays, other multi-level options are summarised on Figure 2. Top left is a single I-bridge of low voltage MOSFETs with the cascade labelled CIB (Cascaded “I” bridge)on the right that control half cycle

waveforms, the high voltage IGBT H-Bridge on the top right provides the uni-polar function. Bottom left is a MOSFET H-Bridge used in each cascaded module of Figure 6.

3 Theory/calculation

3.1 Reference design

For cost, heat flow and mass comparisons, a reference design for a car was chosen with the following characteristics:

1. Peak vehicle power 200kW
2. Four-wheel drive
3. Peak battery voltage per phase of 600V (at nominal battery voltage)
4. Giving a battery phase current of 28A average

The design was evaluated at these key points in the operating envelope:

1. Hill climb, where torque is modulated at near zero motor speed
2. Maximum converter fundamental frequency taken as 250Hz,
   (4ms per rev for single pole)
3. Maximum rate of acceleration, zero to full speed in 10 seconds

The waveform is closely controlled, with one module operating in pulse width modulation (PWM) designated the Module In Control (MIC). Other modules are either in the "off" (short circuit state) or "on" (full battery voltage) state.

3.2 Target costs

In order to normalise cost calculations, Table 1 shows various configurations. Using Li-Ion cells with a nominal 3.6V per cell, the bottom two rows of Table 1 shows a how the PowerElectronicsUK automotive challenge targets for the year 2035 of 50kW/kg and $3/kW (peak power) relate to the reference car design and is used as the target costs in subsequent calculations. It should be noted that the higher the number of cells in each module in the cascade, the higher the cost and weight target and the fewer modules needed per vehicle, although the overall cell count is the same. Also note that the table contains some rounding to allow an integer number of cells to be used. The I-Bridge configuration was only analysed for heat flow and rejected as a result of the power dissipation from the IGBT, as described in section 4.

Table 1, Module cost targets

Vehicle PE mass target		4	kg	
Vehicle PE cost target		£500.00		
Cells per module		**8**	**12**	**16**
Nominal module voltage	V	28.8	43.2	57.6
Modules per phase	#	20	13	10
Total number of modules	#	240	156	120
Target mass per module	g	16	24	32
Target cost per module	£	£2.00	£3.00	£4.00

3.3 PE Cost

As the cost of components change over time, the baseline for cost comparisons was the £GBP price in quantities shown in the volume column on Table 2 as published in the last quarter 2018 by vendors such as Mouser, On-semiconductors and Digikey and are shown below. Costs are split into three main areas:

1. Power MOSFETs
2. Balance of micro-electronics components (BEC)
3. Vehicle installation costs

3.3.1 De-rating rules

There is a trade-off between the amount of de-rating, reliability and cost that is outside the scope of this paper.

A derating of 80% is assumed for the voltage of all semi-conductor devices and a maximum cell voltage of 4V, i.e. 40V devices can work with 8 cells and 80V with 16 cells at 80% derating. Passive components were de-rated at 65%.

3.3.2 MOSFETs

In order to obtain comparisons across different MOSFET voltages and on resistance, a figure of merit F_m is defined:

$$\boldsymbol{F_m = \frac{V_{DS}}{R_{on}.£}} \quad (1)$$

Where V_{DS} = maximum drain source voltage, R_{on} = on resistance at 25 °C in mΩ, £ = volume cost as defined in the cost column.

A higher F_m is better and means that the device has a lower contribution to system cost.

Table 2, Comparison of various semiconductors based on the introduced figure of merit Fm

Device number	Ron Max	Vds	Cost	volume	package	F_m
TPWR8004PL	0.8	40	£1.25	5000	Dsop 5.0×6.0×0.73	40.0
IRLS3034PbF	1.7	40	£0.33	50	TO220	70.6
TPWR6003PL	0.6	30	£5.00		Dsop 5.0×6.0×0.73	10.0
RFB7534PbF	2.4	60	£0.90	1000	TO220, D2Pak	27.9
NDPL18010B	3	100	£5.00		TO220	6.7
FDMS8050ET30	0.65	30	£1.34	1000	Power 56	34.4
IPT015N10N5ATMA1	1.5	100	£2.87	250	PG-HSOF-8	23.2
SUM6003	3.2	80	£1.45	800	D2PAK	17.2
FDD86367	3.3	80	£0.64	5000	TO-252-3	37.7
NTMFS6H800NT1G	1.8	80	£2.12	1500	SO-8FL	21.0
NVMFS6H801N	2.7	80	£0.67	1500	SO−8FL	44.2
NVMFD5C446NL *	2.65	40	£0.61	1500	DFN8	49.7

Marked * are two devices in one package.

The F_m calculation is shown in Table 2. The volume column shows the “numbers off” for the price shown in the cost column (where known). Neglecting BEC, the IRLS3034PbF has the highest F_m at 70.6 but at only 40V V_{DS}. At the higher voltages, the NVMFS6H801N at an F_m = 44.2 performs best.

The TO220 packages require through-hole mountings increasing assembly and hence BEC costs. The other packages are surface mounted at a lower cost but require a more detailed analysis of heat flow as the copper plane forms an integral part of calculations, as described in later sections.
For the I-Bridge configuration high voltage transistors are required for the uni-polar H-bridge completion circuit shown on Figure 2. An IGBT gives the best performance for the completion circuit. Table 3 gives a selection of IGBT costs. Each phase would require 4 IGBTs, 48 per vehicle. This option was not taken any further due to the relatively high heat dissipation (see section 4) requiring liquid cooling or expensive air cooled heat sinks.

Table 3, Comparison of IGBT completion circuit costs

IGBT	V_{CEsat}	V_{CEmax}	Price	Volume	Package
FGH40T65UQDF-F155	1.33	650	£2.34	250	TO247-3
STGP15H60DF	1.6	600	£0.73	1000	TO220

3.3.3 BEC

The Balance of Electronic Components (BEC) costs comprise the following

1. MOSFET drivers (For the topology on Figure 2 right, IGBT drivers are also needed.
2. Micro-controller (if required)
3. Module power supply
4. Isolated communications circuitry
5. Bare printed circuit board (PCB) cost per module is estimated at £0.50 for most options
6. Assembly costs per module estimated at £0.50 for most options
7. Miscellaneous costs, calculated as 10% of the costs of 1 to 6.

3.3.4 Module configuration options

The four module configuration options chosen are summarised on Table 4, module format options considered overall motor control function of Figure 6 is derived from series connected H bridges on Figure 2 There are a multitude of components on the market that would accomplish the BEC function. Each option affects the detail of the system design with merits and de-merits and so a high level analysis using selected options are shown. Finally, an Application Specific IC (ASIC) design is proposed with a set of requirements needed to meet the 2035 targets. Each option is described in more detail in section 3.3.4.2.
The possibility of an MMC [4] configuration, Figure 7 whereby each cell has its own power MOSFETs was explored, however, the current range of MOSFET devices is not optimised for low voltage and hence the costs of this configuration are much higher so the option was not pursued.

Table 4, module format options considered

#	Brief description	Advantages	Disadvantages
O1	Local current control, central feedback	Simple, low bandwidth coms	Unsuitable for larger motors
O2	Centralised motor control	Simpler to design	High bandwidth coms required

O3	Full motor control in each module	Lowest bandwidth coms*	High power micro-controller needed in each module
O4	ASIC	Very low production cost	High development cost

*Coms = the method of communications considered

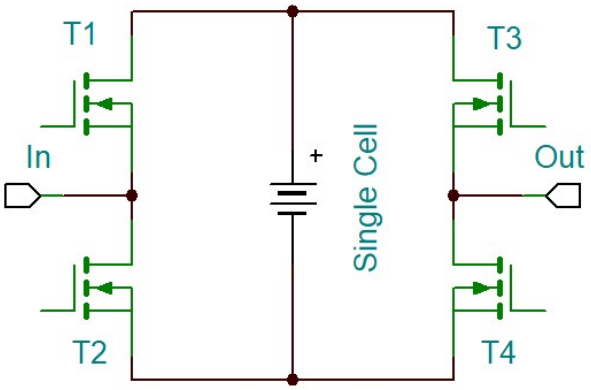

Figure 7, single cell MMC module

3.3.4.1 Inter-module communication (Coms)

As the battery negative of each module varies with the output wave form, any communications (coms) between modules have to be isolated. There are a number of methods available to do this.

1. Coms via the power lines.
2. Wireless
3. Near field
4. Opto-isolation
    a. For direct PWM control
    b. For communications via a serial coms line
5. Capacitor isolation with suitable communications protocol
6. Silicon dioxide isolation layer

The choice of coms will affect the suitability of each option and so is included early in the analysis. Coms via the power lines may be subject of a later paper. The various driver isolation performances have been evaluated in these references[11],[12],[13],[14]. In terms of cost and mass: coms 4a would require at least 2 wires per module from the central controller to each module; 24 in total adding to vehicle installation cost and was not considered further for a production version. The minimum coms cost is dependent on the BOC chosen and is dealt with in each option below.

3.3.4.2 Option O1

An example of an O1 implementation is shown on Figure 8. Coms are very low bandwidth comprising Module in command (MIC), Voltage (V) and frequency (F) demand.

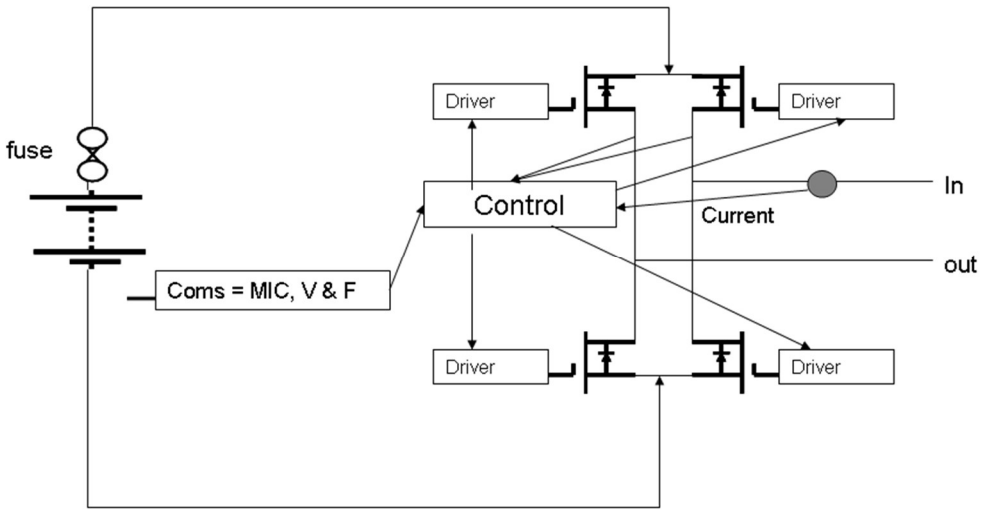

Figure 8. Option 1 module schematic

Control can be performed by devices such as the MC33033 (normally used for "brushless DC" motors), have a high level of integration and the ability to drive High and Low side 3 phases H bridges if required. Such devices operate by comparing the demanded voltage versus winding current on two phases, and control current in an analogue feedback loop from rotor position sensors. Although potentially a cheap solution, this option was not pursued as it was deemed unsuitable for larger automotive traction motors.

Option O2

A typical arrangement for O2 is shown in Figure 9. A centralised motor controller senses all three phase currents and compares with the demanded torque from the vehicle control. Using a standard motor control algorithm [15], Motor Control sends information to each module to generate the appropriate voltage waveform.

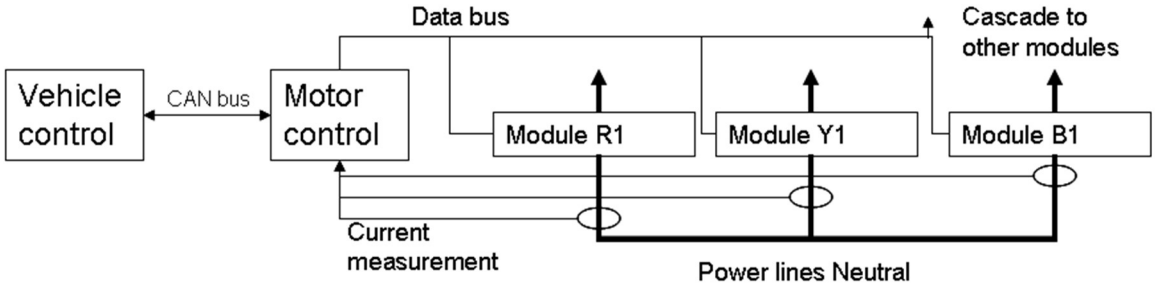

Figure 9, Option 2 configuration

The Data Bus sends duty cycle time from Motor Control to each module and the modules return their internal battery state of charge (SOC). A simple microcontroller computes the SOC for each battery and communicates with the Motor Control via the Data Bus.

Table 5, Costs for option 2 split into 8 and 16 cell derivatives

		O2a 16 cell	O2b 8 cell
Description	**Device**	**Cost**	**Cost**
µC	simple microchip	£0.70	£0.70
Opto isolator control	EL3H7-G	£0.13	£0.13
Full bridge PWM	LM5045	£1.78	£1.78
MOSFET	NVMFD5C446NL		£1.21
	NVMFS6H801N	£2.68	

i2c isolation	ISO1542	£1.73	£1.73
	Components total	£7.03	£5.56
	PCB	£0.50	£0.50
	Assembly	£0.50	£0.50
	Misc	£0.80	£0.66
	Total	£8.83	£7.21
	% target	221%	361%

The system cost is compared with the targets computed earlier and as can be seen from Table 5, the 16 cell configuration is closest to the target but still 221% above target cost.

3.3.4.3 Option O3

By incorporating all the control elements into each module and with common software, the motor control unit of Figure 9 can be removed to save cost. In this option we assume that a more powerful microcontroller can code coms signals using Manchester or similar techniques so that inter-module communications is via simple capacitor isolation, thus removing the need for expensive isolators as shown on Table 6. Again the 16 cell configuration is cheaper at 203% above target cost.

Table 6, Costs for option 3 split into 8 and 16 cellderivatives

Module Costs		**O3a 16 cell**	**O3b 8 cell**
µC	32 bit fast processor	£1.50	£1.50
isolation	Capacitor	£0.20	£0.20
MOSFET Driver	MIC 4604	£1.45	£1.45
MOSFET	NVMFD5C446NL		£1.21
	NVMFS6H801N	£2.68	
Current transducer	CHB-50A	£1.20	£1.20
Total		£7.03	£5.56
	PCB	£0.50	£0.50
	Assembly	£0.50	£0.50
	Misc	£0.10	£0.10
	Total	£8.13	£6.66
	% target	203%	333%

3.3.4.4 ASIC

The target EV market is very large making the viability of an application specific integrated circuit (ASIC) possible. An outline system drawing for an ASIC option is shown in Figure 10.

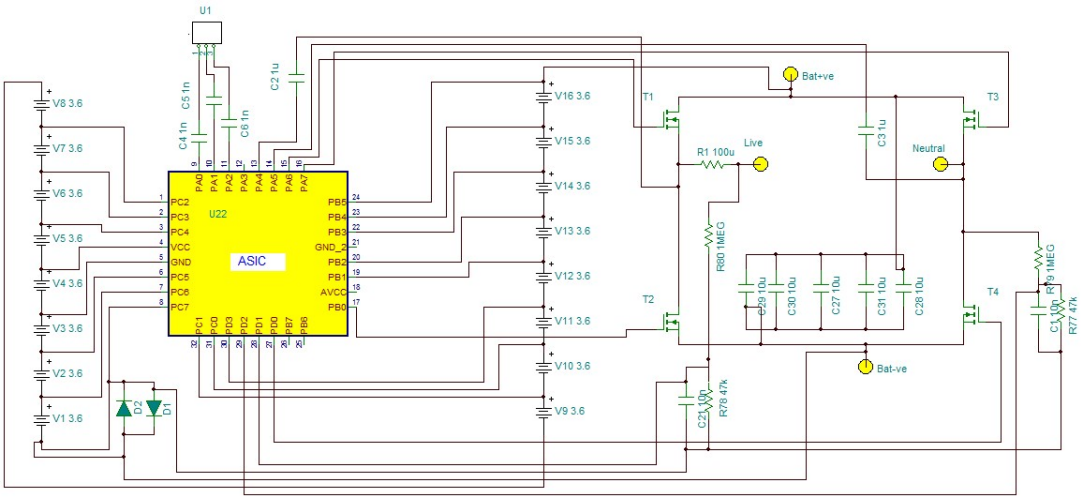

Figure 10, ASIC outline design

The ASIC would contain the MOSFET drivers, power supplies, battery management and encoding for the inter-module coms link via low-cost capacitors C4, C5, C6, each 1nF costs are shown in Table 7. The ASIC cost is based on confidential discussions with a large silicon IC supplier, based on their previous experience the £1.50 cost in very large volume quoted should be achievable. Indeed, large volume manufacturers can negotiate ASIC prices, so the figures below are likely to be an upper price bound.

Table 7, ASIC costs for 16 cell derivative

Module Costs		**ASIC 16 cell**
ASIC		£1.50
isolation	Capacitor	£0.20
Passives		£0.20
MOSFET	NVMFS6H801N	£1.33
Total		£3.23
	PCB	£0.30
	Assembly	£0.30
	Misc	£0.06
	Total	£3.89
	% target	97%

The 16-cell design provides the lowest cost and is below the target. Additionally all the individual cell management features are included, further reducing system cost. An outline ASIC design is shown on Figure 11 and was used to assess the ASIC cost.

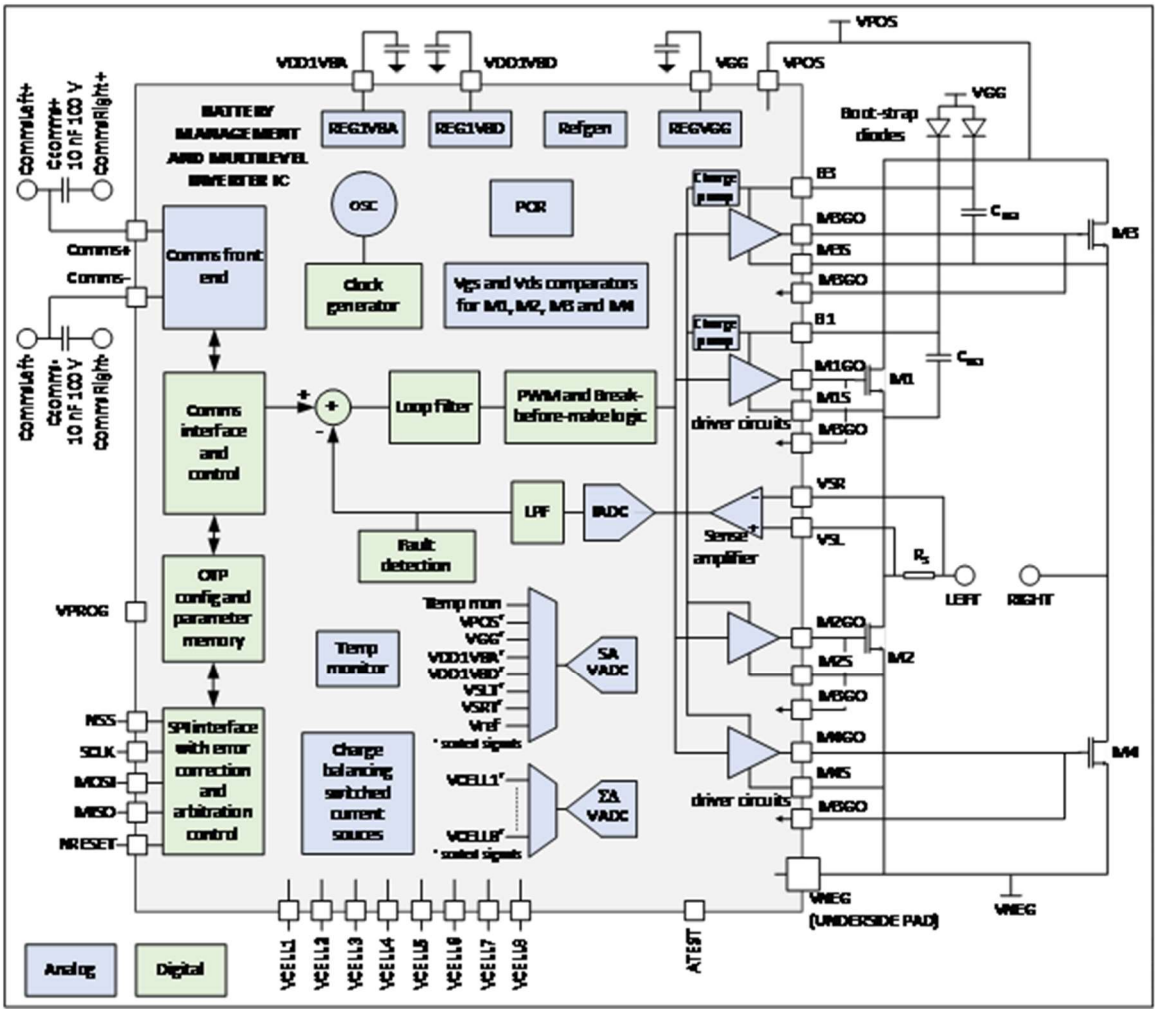

Figure 11, outline ASIC design used for cost comparisons

3.4 Heat flow

3.4.1 MOSFETS

Heat management calculations assume that the entire lower surface of the combined battery pack / PE assembly is made from 3mm thick aluminium plate that acts as both battery housing and a surface from which the heat is dissipated to ambient air. A reference air speed of 30m/s (near the speed limit on an up-hill motorway) is assumed in computing the convective thermal resistance from aluminium to ambient. It is assumed air is drawn through rectangular ducts of height 50mm and width 300mm. For all MOSFETs a PCB copper track is added to the drain in a configuration shown in Figure 12 and H-Bridge placement in Figure 13. It is conservatively assumed that all the heat flow is passed via the metallised drain terminal (shown in grey, Figure 14) and none through the top of the package. The parameters used are: for the MOSFET = NTMFS6H800N data sheet [16] and thermally conductive adhesive = AS1803[17] .

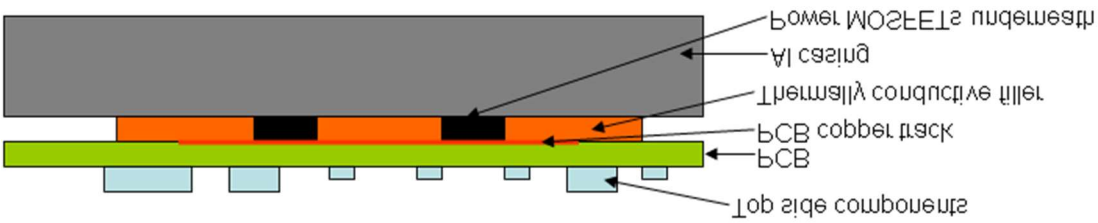

Figure 12, Physical component structure, showing heat flow elements (cross-section representation).

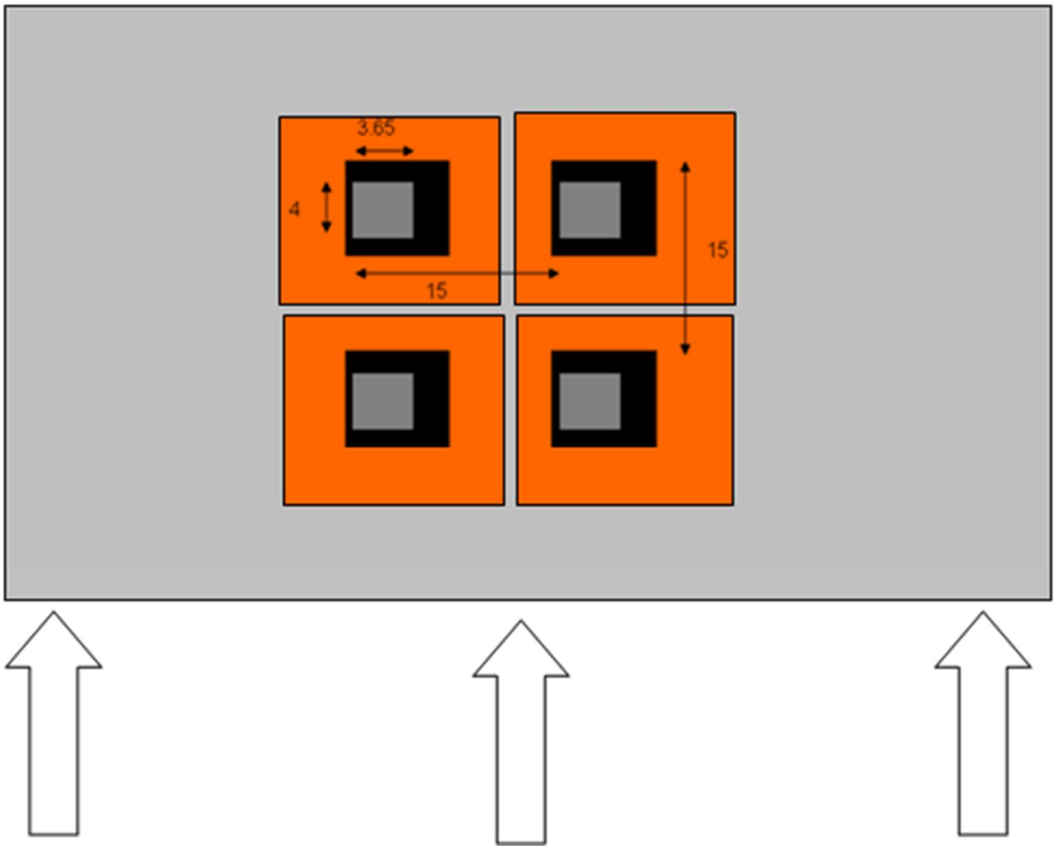

Figure 13. Transparent view of the H-Bridge layout of SO-8FL MOSFET packages. Dimensions shown are in mm.

The four H-Bridge MOSFETs are shown on Figure 13, the grey areas are the metallised drain and black the epoxy case.

T_{cf} = thermal conductivity of the MOSFET epoxy case = 1.55 $\frac{W}{mK}$

This value is so close to the value for the thermally conducting silicone filler that it was assumed that the filler covers the entire underside, and hence the effect of Td was ignored. Each copper square has an area of 2cm^2 and the aluminium plate 80 x 40 mm with uniform air flow in the direction indicated by the arrows.

The thermal resistance from MOSFET to ambient is given by:

$$R\theta_{dtoA} = R\theta_{dDc} + R\theta_{cf}R\theta_{Dc} + \mathrm{R\theta dca} + R\theta_{cf} + R\theta_{fAl} + R\theta_{AlA} \qquad (2)$$

Where the thermal resistances are:

$R\theta_{dca}$ device (junction) to case = 0.75 °C/W (from data sheet)

$R\theta_{cca}$ average resistance from case to copper

$R\theta_{cf}$ copper through filler, $R\theta_{fAl}$ filler to Aluminium plate and $R\theta_{AlA}$ is the convective thermal resistance from the aluminium plate to ambient.
At full power and R_{on} typical = 2.1Ω at 28A average with i^2R = 1.6Wth thermal per device gives 3.3Wth per H-bridge, (Wth = heat flow in Watts thermal.) with a junction temperature of 25C. At the working junction temperature R_{on} = 4.2 Ω giving 6.6Wth of heat.
Where:
w_{cu} = width of the copper layer = 70µm,
w_{al} = width of aluminium casing = 3 mm
A_{cu} = area of the copper underneath each MOSFET = 2cm^2.
Metal thermal resistances were evaluated using a worst-case approximation as shown on Figure 14.

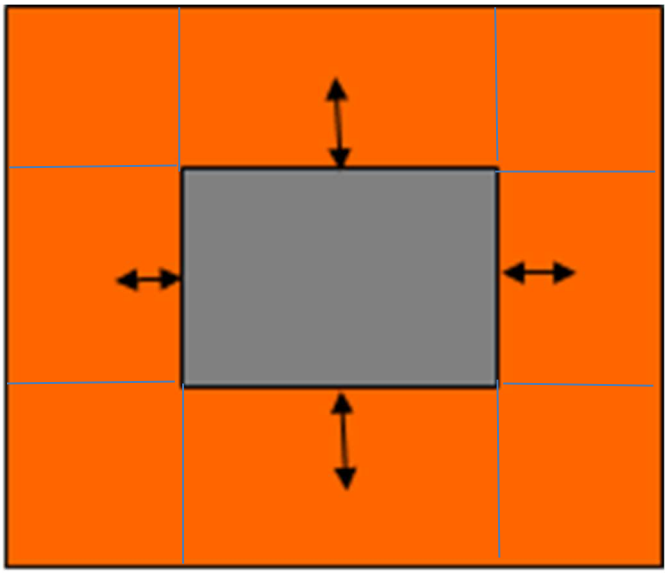

Figure 14, heat flow approximation

The central grey area is assumed to be at a uniform temperature, and the arrows length *L* show half the distance from this central region to the metal periphery.

$$R\theta = \frac{0.25}{\rho WT} \quad (3)$$

Where *T* is the metal thickness and *W* is the width of the upper (grey) metal. The beneficial effects of the outer 4 squares are ignored, so there are 4 thermal paths in parallel hence the 0.25 constant.

Figure 15. Approximation method used to evaluate metal thermal resistance

For the copper layer ρCu = 401 W/m.K, *L* = 1.675 *W* = 4 *T*= 0.075 mm
giving
$R\theta_{cca}$ = 3.481 C/W (4)

For the filler layer, ρF = 2 W/m.K
L = 1, *W* = 4 *T* = 3 mm giving

$R\theta_{cf}$ = 2.604 C/W (5)

and aluminium ρAl = 237 W/m.K
L= 8, *W* = 28 T= 3 mm giving

$R\theta_{fAl}$ = 0.1 C/W (6)

Thermal resistance from MOSFET junction to aluminium plate = 5.2 C/W
Thermal resistance from plate to air was computed assuming a duct with fully developed flow (being the worst-case condition). Input data is shown on Table 8.

Table 8, duct input data used in computations

Duct height	0.05	m
Duct width	0.3	m
Duct area	0.015	m^2
Duct perimeter	0.7	m
Hydraulic diameter	0.09	m
Air pressure	101325	Pa
Air temperature	313	K
Air density	1.13	kg/m3
Prantl no	0.707	
Viscosity	1.85E-05	Ns/m2
Arc conductivity	0.0263	

Table 9. Results of air flow thermal analysis

Velocity, m/s	Re	NuD	W/m^2K
5	26187	71	21.8
10	52374	124	37.9
15	78560	171	52.4
20	104747	215	66.0
25	130934	257	78.9
30	157121	298	91.3

Where Re = Reynolds number
NuD = Nusselt number
h = the average thermal conductivity
using the Dittus Boelter[18] method.

At 30 m/s h = 91.3 W/m^2K and assuming the convective surface is a square of 40mm x 40mm,
$R\theta_{AlA}$= 6.85 C/W (7)

Total thermal resistance from junction to air is therefore 12 C/W and with 6.6Wth gives a junction temperature of 139C under the assumed worse case condition at 40C ambient

temperature. This is well within the maximum of 175^0C quoted in the NTMFS6H800N data sheet.

3.4.2 I-Bridge completion circuit

Heat flow per device is given by: $0.5\ I_{av}VCE_{sat}$

Where VCEsat is the transistor saturation voltage at the average current I_{av}.

For the STGP15H60DF IGBT, this give a heat flow of 22.4W. As this would require a significant heat sink, and nullify some of the benefits of the concept, this option was not taken any further.

3.5 Mass

In order to make mass comparisons, the following assumptions were made:

1. Module interconnections were excluded as conventional systems also require battery interconnects.
2. Because the interconnections are dual function, current / heat spreader no allowance is made for heat management off the PCB.
3. PE aluminium casing (the passive heat sink) is excluded
4. Battery management connections are excluded.
5. Only PCB and component masses are included.

A PCB for option O2a (the best non-ASIC solution) was built (this being typical of all the options) and weighed at 35g. A mock-up of an ASIC PCB weighed 5g. There are 10 modules per phase and 4 motors in the reference design giving 120 modules in total, the mass is shown on Table 10 and it can be seen that the ASIC solution is nearly 7 times lighter than the target and assuming air cooling.

Table 10, Mass comparison with target.

2035 target = 50 kW/kg, number of modules = 120

Item	Unit	Best non-ASIC	ASIC
PCB module	g	35	5
Vehicle PE	kg	4.2	0.6
% target		105%	15%

4 Discussion and Results

4.1 Cost and Mass

A number of system configuration options were designed to compute overall costs and compared with the 2035 target costs to give a percentage of target as summarised in Table 11. Devices currently available for BEC tend to be cheaper for system voltages up to 40V (8 cells), above that costs increase due to considerations in the basic silicon design. However, it is clear from the results that the reductions are insufficient to offset the increased number of modules required for the lower voltage modules. In all cases the 16 cell option gives the cheaper overall system cost.

Table 11, Cost summary across options.

Cost relative to 2035 target		
	16 Cell	8 cell
O2	203%	333%
O3	221%	361%
ASIC	97%	N/A

4.1.1 ASIC

In the ASIC option, the PCB and assembly costs are reduced as the components are minimal so saving costs. In addition the ASIC contains all the BMS circuitry further reducing system costs below and beyond the 2035 cost targets.

4.2 General discussion

So far, this paper has concentrated on the impact of CHB on the vehicle. CHB has many other benefits external to the vehicle; under certain circumstances, battery charging can be from single or three phase mains, DC low impedance source (for example a fast charger) and Photovoltaic arrays (PV) [19]. There is also considerable interest in using vehicle batteries for mains grid stabilisation [20].

If the minimum battery voltage is greater than the peak mains voltage and the CHB is synchronised with the mains, then batteries can be charged with single or three phase supplies without the need for additional chargers. In addition, if the software includes MPPT algorithms, then batteries can be charged directly from PV cells as long as the PV array voltage is higher than an individual module voltage.

Wide use of CHB would then remove the need for external chargers and enable more rapid adoption in developing countries where mains supplies are sporadic but there is plenty of sunlight for PV vehicle charging. These country wide cost reductions would make a significant contribution to EV uptake.

This paper has only concentrated on traction control of EV motors, vehicle also have to power ancillaries. There are many techniques available to do this but are outside the scope of this paper.

5 Conclusions

Electric Vehicles are seen as a major contributor to reducing carbon emissions and hence global warming. The PowerElectronicsUK Automotive Challenge road map outlines reductions in cost and mass for the power electronics that control EV motors as on driver for longer range and hence quickening EV uptake. This paper has shown that from a cost and mass perspective of the vehicle alone, CHB can meet the 2035 targets with a special ASIC. Design houses quote about 18 months to 2 years to make prototype ASICs, meaning that a solution could be available in 2023 if funds were made available, 12 years earlier than the target date. Additionally, vehicle installation is simpler due to passive cooling, EV range is increased due to the higher efficiency of CHB and power electronics in external charging facilities are not required reducing off-vehicle costs by more than an order of magnitude.

The paper shows that the new topology itself reduces mass and cost becoming even more beneficial when the effects of cooling systems are removed.

Acknowledgements

We thank The PowerElectronicsUK Automotive Challenge network funded by EPSRC for this work through the BIPED feasibility study.

6 References

[1] Paul Taylor. Power Electronics UK n.d. https://www.power-electronics.org.uk/.

[2] Chang F, Ilina O, Lienkamp M, Voss L. Improving the Overall Efficiency of Automotive Inverters Using a Multilevel Converter Composed of Low Voltage Si mosfets. IEEE Trans Power Electron 2019. doi:10.1109/TPEL.2018.2854756.

[3] Mukherjee N, Tricoli P. A state-of-charge equalisation technique of super-capacitor energy storage systems using sub-module DC-DC converter control within modular multilevel converter (MMC) for high speed traction drive applications. Proc. Univ. Power Eng. Conf., 2015. doi:10.1109/UPEC.2015.7339948.

[4] Quraan M, Yeo T, Tricoli P. Design and Control of Modular Multilevel Converters for Battery Electric Vehicles. IEEE Trans Power Electron 2016. doi:10.1109/TPEL.2015.2408435.

[5] Davidson CC, Trainer DR. Innovative concepts for hybrid multi-level converters for HVDC power transmission, 2011. doi:10.1049/cp.2010.0982.

[6] Tolbert LM, Peng FZ, Habetler TG. Multilevel converters for large electric drives. IEEE Trans Ind Appl 1999. doi:10.1109/28.740843.

[7] Tolbert LM, Peng FZ, Cunnyngham T, Chiasson JN. Charge balance control schemes for cascade multilevel converter in hybrid electric vehicles. IEEE Trans Ind Electron 2002. doi:10.1109/TIE.2002.803213.

[8] Chang F, Zheng Z, Li Y. PWM strategy of a novel cascaded multi-level converter for battery management. 2014 17th Int. Conf. Electr. Mach. Syst. ICEMS 2014, 2015. doi:10.1109/ICEMS.2014.7014045.

[9] Du Z, Ozpineci B, Tolbert LM, Chiasson JN. DC-AC cascaded H-bridge multilevel boost inverter with no inductors for electric/hybrid electric vehicle applications. IEEE Trans Ind Appl 2009. doi:10.1109/TIA.2009.2018978.

[10] Hohm DP, Ropp ME. Comparative study of maximum power point tracking algorithms. Prog Photovoltaics Res Appl 2003. doi:10.1002/pip.459.

[11] Ye Z, Pilawa-Podgurski RCN. A power supply circuit for gate driver of GaN-based flying capacitor multi-level converters. WiPDA 2016 - 4th IEEE Work. Wide Bandgap Power Devices Appl., 2016. doi:10.1109/WiPDA.2016.7799909.

[12] Timothe S, Nicolas R, Jean-Christophe C, Jean-Daniel A. Design and characterization of a signal insulation coreless transformer integrated in a CMOS gate driver chip. Proc. Int. Symp. Power Semicond. Devices ICs, 2011. doi:10.1109/ISPSD.2011.5890865.

[13] Jasielski J, Kuta S. Applied methods of power supply and galvanic isolation of gate drivers of power transistors in bridging end stages of Class D amplifiers and inverters. Sci Technol Innov 2018. doi:10.5604/01.3001.0012.1413.

[14] Nguyen VS, Lefranc P, Crebier JC. Gate Driver Supply Architectures for Common Mode Conducted EMI Reduction in Series Connection of Multiple Power Devices. IEEE Trans Power Electron 2018. doi:10.1109/TPEL.2018.2802204.

[15] Nakao N, Akatsu K. Vector control specialized for switched reluctance motor drives.

Electr Eng Japan (English Transl Denki Gakkai Ronbunshi) 2016. doi:10.1002/eej.22776.
[16] Semiconductors O. NTMFS6H800N DataSheet n.d. https://www.onsemi.com/PowerSolutions/product.do?id=NTMFS6H800N (accessed July 17, 2019).
[17] Silicones A. AS1803 Thermally conductive adhesive n.d. https://docs-emea.rs-online.com/webdocs/0b64/0900766b80b644dd.pdf (accessed July 17, 2019).
[18] Dittus FW, Boelter LMK. Heat transfer in automobile radiators of the tubular type. Int Commun Heat Mass Transf 1985. doi:10.1016/0735-1933(85)90003-X.
[19] Vavilapalli S, Umashankar S, Sanjeevikumar P, Ramachandaramurthy VK, Mihet-Popa L, Fedák V. Three-stage control architecture for cascaded H-Bridge inverters in large-scale PV systems – Real time simulation validation. Appl Energy 2018. doi:10.1016/j.apenergy.2018.08.059.
[20] Yu M, Huang W, Tai N, Zheng X, Wu P, Chen W. Transient stability mechanism of grid-connected inverter-interfaced distributed generators using droop control strategy. Appl Energy 2018. doi:10.1016/j.apenergy.2017.08.104.